

Classification of UAVSAR Polarimetric Data for Wildfire Monitoring

Author: Wen Tao Lin¹

Mentors: Karen An and Charles Z Marshak²

¹Case Western Reserve University

²Jet Propulsion Laboratory/California Institute of Technology

Abstract

Wildfires are an ongoing threat to communities due to climate change. They are characterized by their unpredictability and can lead to severe consequences if not handled appropriately. Remote sensing can significantly contribute to wildfire monitoring by providing image data over large areas of land. Uninhabited Aerial Vehicle Synthetic Aperture Radar (UAVSAR) is a type of active radar sensor well-suited for assessing forest structure due to its ability to penetrate the atmosphere under most conditions. We utilize the polarimetric data collected from UAVSAR's L-band radar to detect burn scars and classify fire perimeters. The polarimetric data provides valuable insights into the land's scattering properties, which exhibit remarkable sensitivity to forest fuel load, a key indicator for fire burn scars and vegetation burn severity. Using classification techniques, we automate the generation of fire perimeters and burn severity maps, reducing the manual efforts required. This product will enable real-time wildfire monitoring by providing timely updates to aid disaster response and serve as a prototype for future research in wildfire classification using UAVSAR data.

Background

With climate change creating warmer temperatures and drier conditions, wildfires are becoming more prolonged and exhibiting greater activities [1]. As a result, the consequences of wildfires are getting more extreme and pose a greater threat to our communities. These consequences include habitat destruction (leading to biodiversity loss), air pollution (increasing the risk of respiratory problems), soil degradation (reducing agricultural productivity), and many

more [2]. As technology advances, more tools are being developed to offer additional wildfire surveillance by identifying areas at high risk and allowing appropriate disaster response. One of many technologies available is remote sensing, the acquisition of Earth's information from a distance through electromagnetic waves [3]. Remote sensing provides quantitative information of the target area, which allows for fire behavior analysis and fire management to mitigate the risk.

We utilize the data collected from NASA's Uninhabited Aerial Vehicle Synthetic Aperture Radar (UAVSAR) L-band synthetic aperture radar, which is a type of active radar sensor well-suited for assessing forest structure due to its ability to penetrate the atmosphere under most conditions, including cloud and smoke [4]. UAVSAR's polarimetric data from previous SAR Wildfire studies exhibit remarkable sensitivity to forest fuel load, as they can capture the changes in forest structures resulting from fires [5]. By comparing pre- and post-fire polarimetric data, we can detect burn scars and map soil burn severity to facilitate post-fire recovery.

With the advancement of remote sensing, fire perimeter mapping has evolved from manual mapping via Global Positioning System (GPS) to automated mapping via satellite imagery to improve accuracy, as manual mapping is often affected by low visibility and unreachable areas [6]. We develop a product to automate the UAVSAR-based mapping of fire perimeter and soil burn severity, improve the manually mapped output, and reduce the effort of fire mapping to aid disaster response in a timely-matter. With the generated fire perimeter and burn severity, local enforcement will have more information to guide their decision-making process during and after the fire.

This study focuses on three wildfires that occurred in the Los Angeles, California area: Bobcat (2020) – burned over 115,000 acres, La Tuna (2017) – burned over 7,000 acres, and Station (2009) – burned over 160,000 acres. Bobcat and Station fires are chosen as an extension to An et al.’s research in 2023 on wildfire detection and monitoring with L-Band Polarimetric SAR [5]. Meanwhile, La Tuna Fire is chosen as a third, smaller scaler, fire to compare the outputs to and use as a sample fire for the product tutorial on GitHub.

Data

The raw data used is collected from polarimetric L-band SAR (PolSAR), which has a strong capability to penetrate forest canopy, allowing for more interactions between the radar signal and the tree structures. PolSAR can collect signals in different polarizations, where the horizontal polarization is indicated as H and the vertical polarization is indicated as V. By controlling the emitting and receiving polarization of signals, various information can be collected from the different scattering mechanisms in a wildfire area resulting from different combinations of horizontal and vertical radar waves (HH, VV, HV, VH) [7].

The final product specifically focuses on the HV cross-polarized images to analyze volume scattering, which is caused by the leaves and branches in a forest canopy. Volume scattering has a positive correlation with vegetation, such that higher HV values are associated with higher fuel load because the signal must interact with more canopy components before returning to the sensor [8]. Therefore, a comparison of the HV values before and after a fire is a good factor to measure the fire perimeter and burn severity, as negative greater change in HV can be associated with greater burn severity. The product uses the Log Ratio between pre- and post-fire images as a method for change detection [9].

For the case studies of the three fires, the following UAVSAR flight line and dates are used [10]:

Fire Name	Pre-Fire	Post-Fire
Bobcat 09/06/2020 – 12/18/2020	SanAnd_08525 on 10/11/2018 SanAnd_08527 on 02/05/2018	SanAnd_08525 on 11/17/2021 SanAnd_08527 on 10/14/2020
La Tuna 09/01/2017 – 09/09/2017	SanAnd_08525 on 10/23/2014	SanAnd_08525 on 11/02/2017
Station 08/26/2009 – 10/16/2009	SanAnd_08525 on 02/27/2009 SanAnd_08527 on 02/27/2009	SanAnd_08525 on 03/03/2010 SanAnd_08527 on 04/15/2010

Table 1. Flight line and date used for case study on Bobcat, La Tuna, and Station Fires.

Due to the size of the Bobcat and Station Fires, two UAVSAR flight lines (SanAnd_08525 and SanAnd_08527) are used for both fires to cover the region of and around the fires. Because there are two flight lines, the dates of the flights are selected as close as possible to ensure data consistency when merging the perimeters from each flight line into one single fire perimeter. However, at the time of this study, there is no post-fire UAVSAR data available for the north region (SanAnd_08527) of the Bobcat Fire. As a result, we use an active fire data set for that half of the fire region. The latest pre-fire flight that covers La Tuna Fire location is also three years before the fire.

Output

By comparing our UAVSAR-based mappings with the published Landsat-based mapping of fire perimeter and burn severity from the US Forest Service's Monitoring Trends in Burn Severity Program (MTBS), we can assess the accuracy of our outputs using the published maps as baseline [11]. The dates for the pre- and post- fire data used by MTBS is unknown, which

means that the two products likely have different dates and could thus result in differences between outputs. Our final products are GIS-compatible for spatial analysis: the perimeter is outputted as a GeoJSON file and burn severity is outputted as a GeoTIFF file. For this study, Bobcat Fire is used as the primary fire for method research, as it is the most recent fire out of the three.

Fire Perimeter Comparison

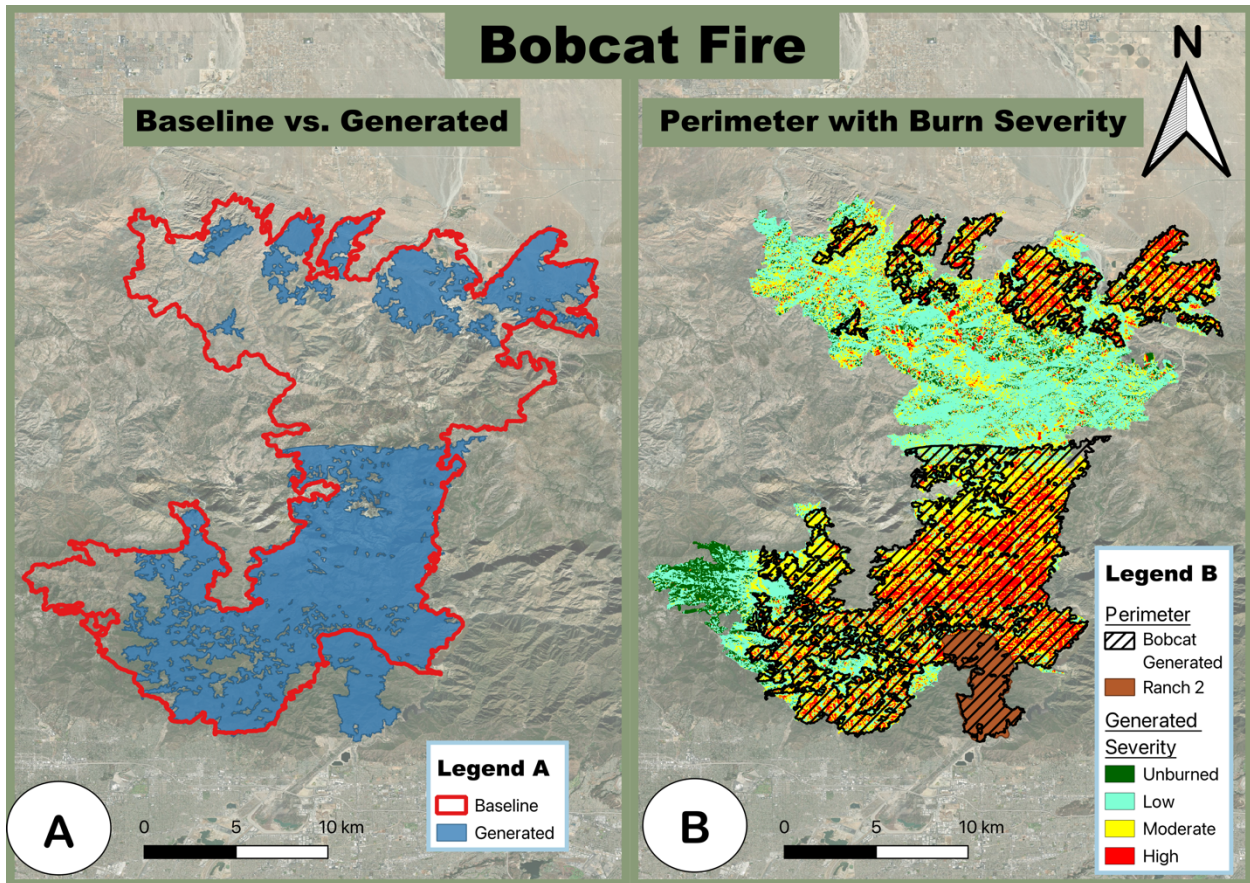


Figure 1. Comparison of the product generated Bobcat Fire perimeter with the MTBS baseline perimeter (A) and the product generated burn severity map with interpolation (B). Refer to Table I for the pre- and post-fire dates for UAVSAR data.

The output perimeter for the Bobcat Fire is overlayed with the published perimeter from MBTS in *Figure 1A* to capture the general shape of both perimeters. Due to the lack of post-fire data for the northern region, a full fire perimeter is not available. As a result, most of the northern fire area is missing from the generated perimeter. However, the generated perimeter in

Figure 1A raises a concern: the fire started in the south, so there should be a path from the south to the north since the fire has to travel, even if the north is only presented with active fire data. This is likely because the fire is more severe in the upper half of the north as shown in the burn severity maps in *Figure 3A & 3B*, as well as a user-specified minimum area size to filter out small shapes (the min size is 1 square kilometer for the generated Bobcat perimeter). As a result, some parts of the path might have been filtered out due to their size, while others are classified as non-fire due to the low log-ratio value used for change detection.

Additionally, the generated perimeter does not cover the entire baseline perimeter. By comparing the generated perimeter with the generated burn severity with interpolation (filling in the missing values from the original UAVSAR data), much of the generated perimeter corresponds to the areas with moderate and high burn severity. Meanwhile, the unburned and low burn severity areas are classified as non-fire by the algorithm, and will, therefore, not be part of the output perimeter. Moreover, there is a small false positive region at bottom (*Figure 1A*). This is because another wildfire, Ranch 2 (08/13/2020 – 10/05/2020), was occurring around the same timeframe as Bobcat (09/06/2020 – 12/18/2020), and the dates of the UAVSAR's SanAnd_08525 line (10/11/2018 - 11/17/2021) used for Bobcat also overlapped Ranch 2's date. The brown polygon in *Figure 1B* outlines the published Ranch 2 perimeter by the MTBS, and the polygon covers the entire false positive region of Bobcat's perimeter.

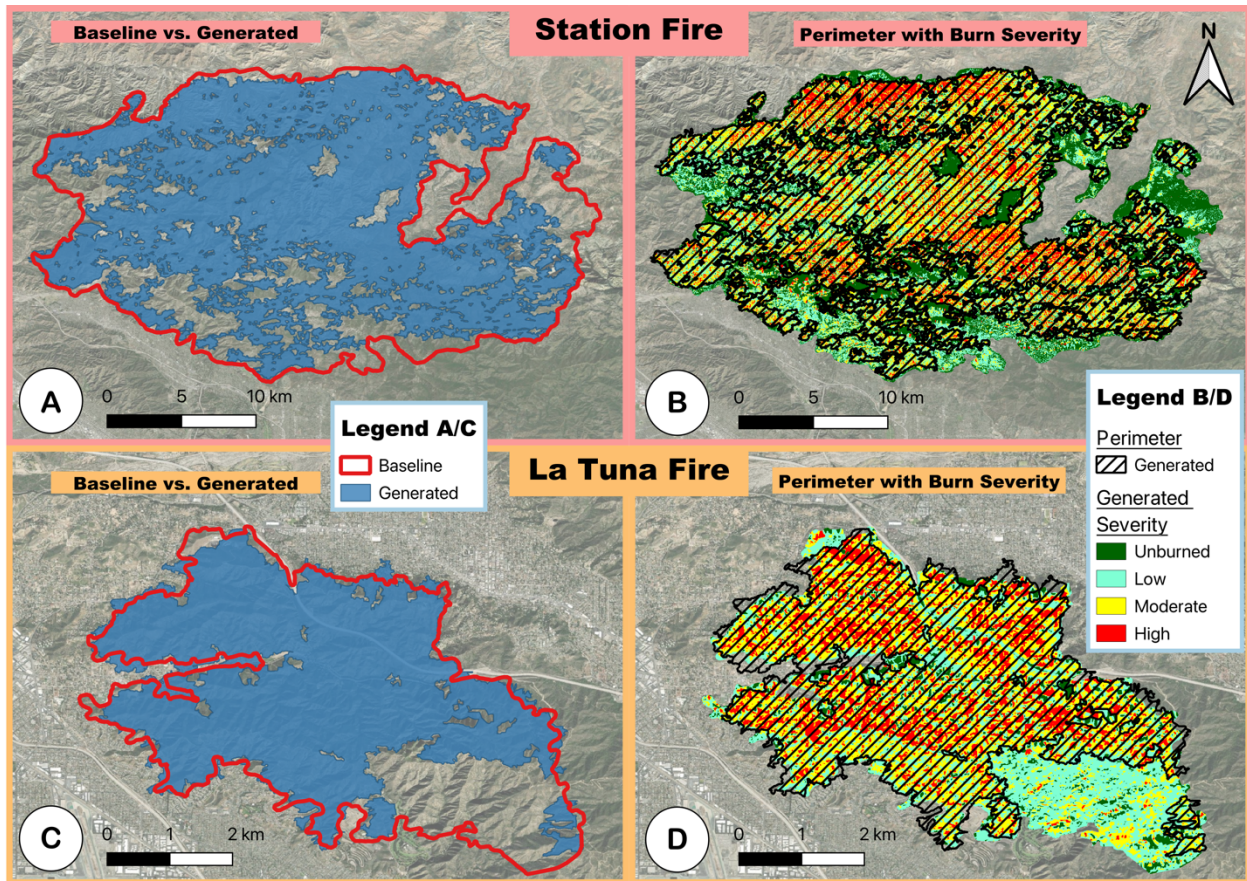


Figure 2. Comparison of the product generated Station/La Tuna Fire perimeters with the MTBS baseline perimeter (A, C) and the product generated burn severity maps with interpolation (B, D). Refer to Table 1 for the pre- and post-fire dates for UAVSAR data.

To further assess the model pipeline's performance on perimeter-generation, it is also used to generate the perimeters for the Station and La Tuna fires as shown in *Figure 2*. The performance is like that of Bobcat's, where the general fire shape is captured but the unburned/low severity areas are left out of the generated perimeters.

Burn Severity Comparison

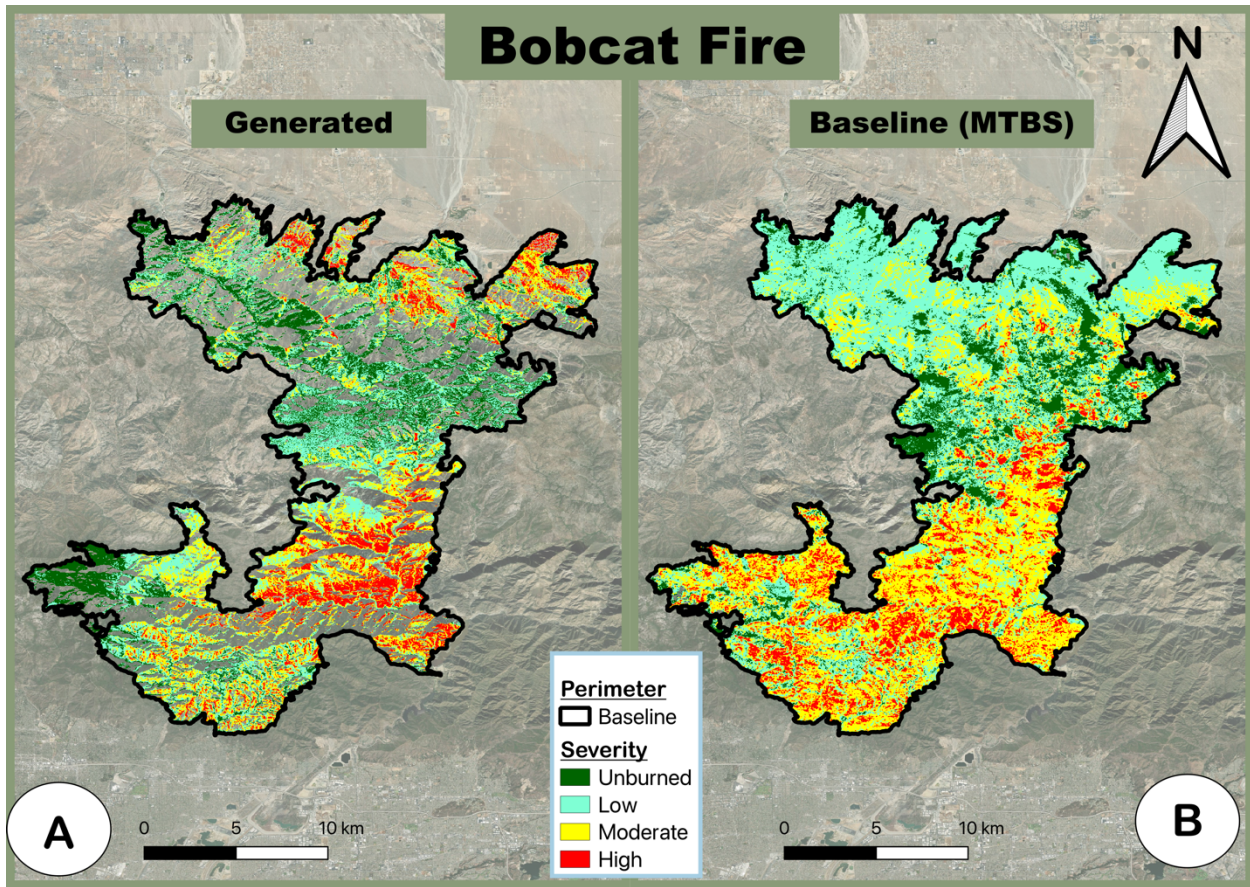


Figure 3. Comparison of the product generated Bobcat Fire burn severity map without interpolation (A) with MTBS baseline burn severity map (B). Refer to Table 1 for the pre- and post-fire dates for UAVSAR data.

A side-by-side comparison of the generated Bobcat burn severity map and the MTBS published Bobcat burn severity map is shown in *Figure 3*. Like with the generated perimeter, the lack of post-fire data in the north also affects the burn severity map. Moreover, the missing values in the UAVSAR image are not interpolated for the burn severity to prevent inaccurate severity classification. The current method to interpolate the missing value is by assigning the value of the nearest pixel, which could greatly affect the severity map depending on the scale of the missing values. In the case of UAVSAR flights over terrain areas, this interpolation approach is not ideal, as the scale of the missing data is too large, so an entire burn severity class could be omitted in a region with high prevalence of another class. This product, however, does provide

the user with an option to decide if they want to generate a burn severity map with or without interpolation. The burn severity maps in *Figure 1 & 2* are generated with interpolation, while the maps in *Figure 3 & 4* are generated without interpolation.

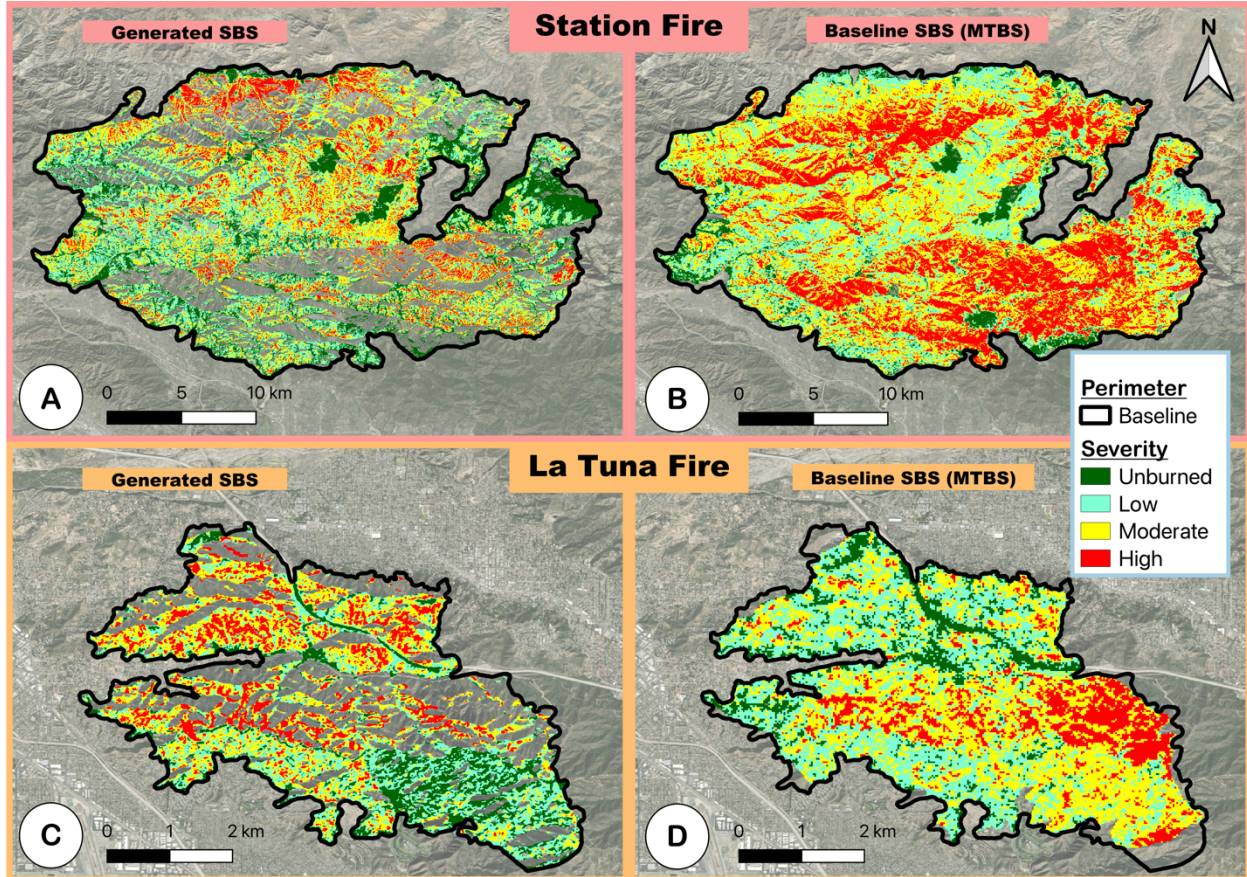


Figure 4. Comparison of the product generated Station/La Tuna Fire burn severity maps without interpolation (A, C) with MTBS baseline burn severity maps (B, D). Refer to Table 1 for the pre- and post-fire dates for UAVSAR data.

By inspecting the Bobcat (*Figure 3*), Station (*Figure 4A & 4B*), and La Tuna (*Figure 4C & 4D*) severity maps, we can see that the current approach is able to capture most of the unburned areas (shown in dark green) according to the baseline maps. However, there seems to be a disagreement for the thresholds to classify low, moderate, and high severity between the generated and baseline severity maps. This is likely due to the different type of data used. The baseline maps from MTBS are developed using Landsat's optical data, while our products are developed using UAVSAR's radar data. The optical sensor is sensitive to visible and infrared

light, which enables detailed land cover analysis [12]. MTBS's burn severity mapping utilizes differenced Normalized Burn Ratio (dNBR), which measures the changes in greenness after a fire based on the optical images. On the other hand, radar sensor can penetrate cloud cover, and UAVSAR, specifically, can penetrate through vegetation, which enables vegetation structure analysis. Our product utilizes the HV Log Ratio, which detect the changes in shape and moisture properties of an area after fire [8].

Moreover, the thresholds to discriminate between burn severity classes used in MTBS' map are subjective and dependent on their analysts' interpretation. Meanwhile, our product's thresholds are determined using K-Means algorithm to divide the HV Log Ratio values into the four classes of roughly equal size [13][14].

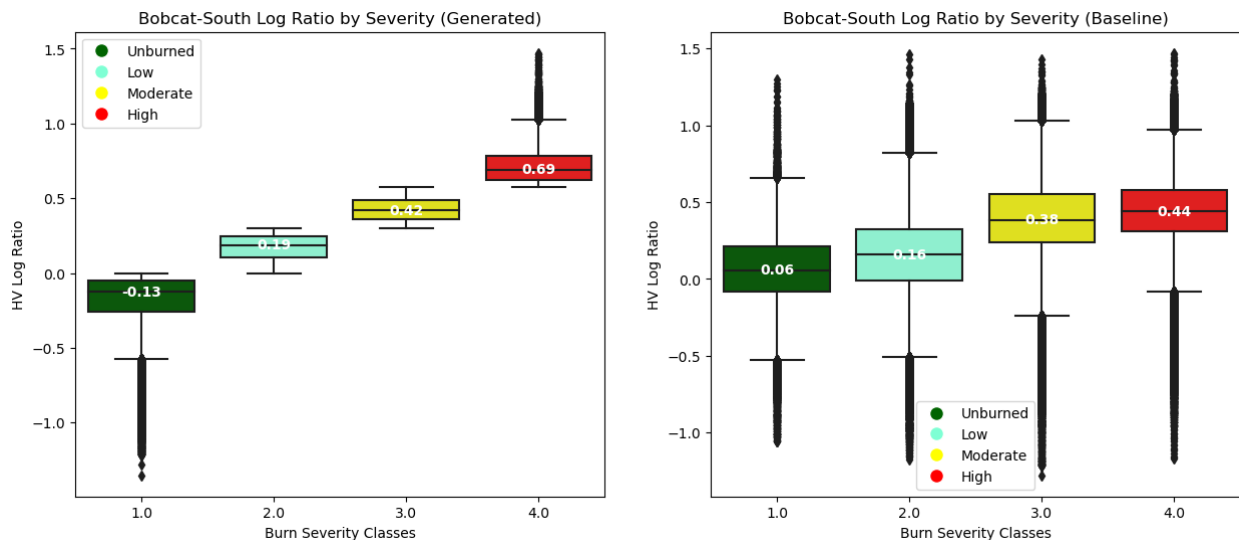


Figure 5. HV Log Ratio distribution by burn severity for Bobcat Fire (South) shown in boxplots. The Log Ratios in the left boxplot are sorted by the generated severity classes, while the values in the right boxplot are sorted by the baseline severity classes. The median log ratio value for each class indicated in the center in white.

Figure 5 above shows a side-by-side log ratio distribution for Bobcat Fire (South) sorted by both generated and baseline burn severity classes. The generated severity plot shows a clear division of the thresholds between the four burn severity labels, while the baseline plot shows overlapping log ratio values for different severity classes. The poor log ratio distribution of the

MTBS's severity map is likely due to the different measurement used between the two products, as described earlier.

Methods

All the figures shown below is associated with the South region of Bobcat fire.

Radiometric Terrain Correction

UAVSAR is a side-looking SAR instrument, which means data are collected via an incidence angle. As a result, this leads to geometric and radiometric distortions, particularly in areas with varying surface slopes [5]. In order to improve the backscatter estimate and remove geometric distortion, a radiometric terrain correction algorithm (RTC) is applied to the raw HV multi-look cross (mlc) product slant range images [15]. However, when a radar signal encounters a terrain feature, such as a hill, that obstructs the signal's path to the ground, it creates shaded areas known as "radar shadow." These shaded areas often lack backscatter, so the radiometric correction cannot be applied here. The RTC algorithm will remove these radar shadows for the user to indicate as missing values [15].

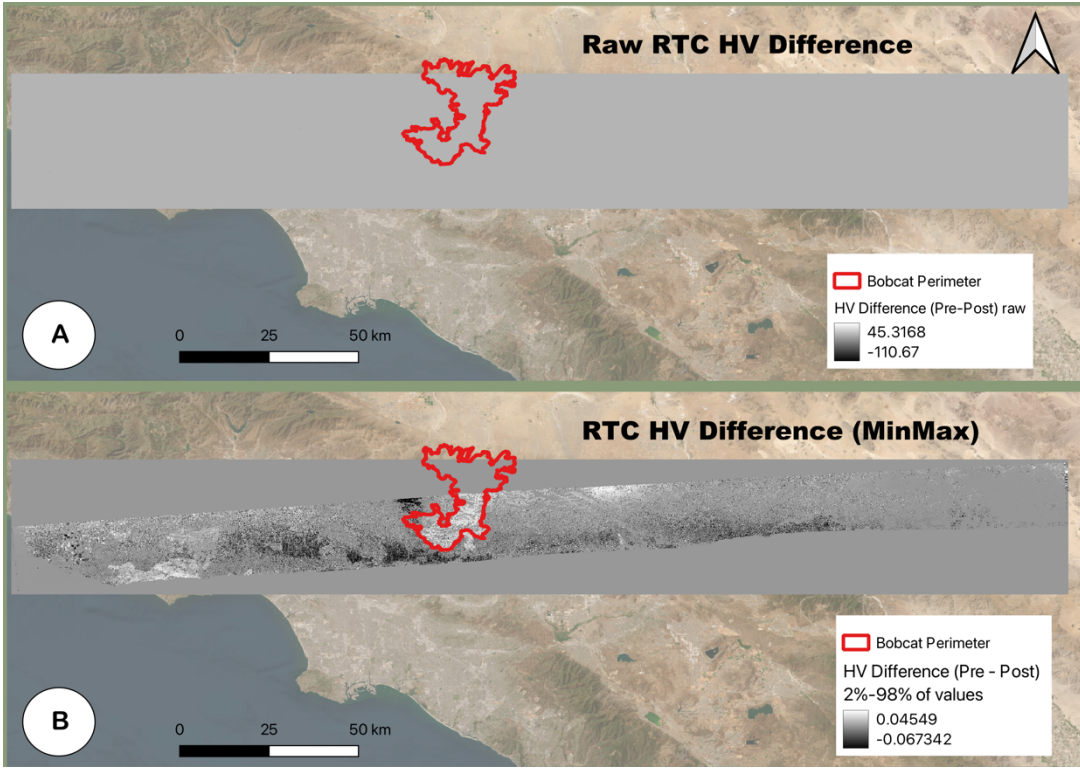


Figure 6. HV difference for Bobcat South flight line after RTC (A). Scaled difference to only the middle 96% (B).

Data Preparation

Cropping & Clipping

To manage the extensive coverage area in UAVSAR flights shown in *Figure 6*, our product prompt the user to crop UAVSAR images into a circular shape. The user has the flexibility to specify the center coordinates of the circle and the desired radius in kilometers, and the image will be cropped based on the intersection of the circle and the original image. This aims to optimize the memory usage and run time of the product by enabling users to focus on processing specific areas of interest. Additionally, the raw radiometric corrected image often contains outliers that affect the visibility of the overall image (*Figure 6A*), which could be improved by performing a simple clipping to remove outliers (*Figure 6B*).

Interpolation

Due to the radar shadows from terrain features, the post-RTC data will contain missing values. In order to capture the perimeter edges, the nearest neighbor interpolation algorithm is applied to fill in the missing values with their nearest valid values [16]. This approach is selected due to fire's nature to spread outward, since burned areas are generally connected. However, due to concerns for inaccurate interpolation, the burn severity mapping is not generated using interpolated images as discussed in the *Burn Severity Comparison* section above. On the other hand, the fire perimeter mapping is generated using interpolated images because this method allows for a more forgiving margin of error. This is primarily because we are simplifying the problem to classify into two classes (fire and non-fire) instead of four (the burn severity labels). As a result, even if the interpolated values deviate somewhat from their true values, they should still align relatively closely, given the interconnected nature of fires. This interconnectedness ensures that the classification of fire and non-fire pixels remains reasonably accurate. By interpolating missing values, this allows us to capture the maximum extent of the burned areas.

Despeckling

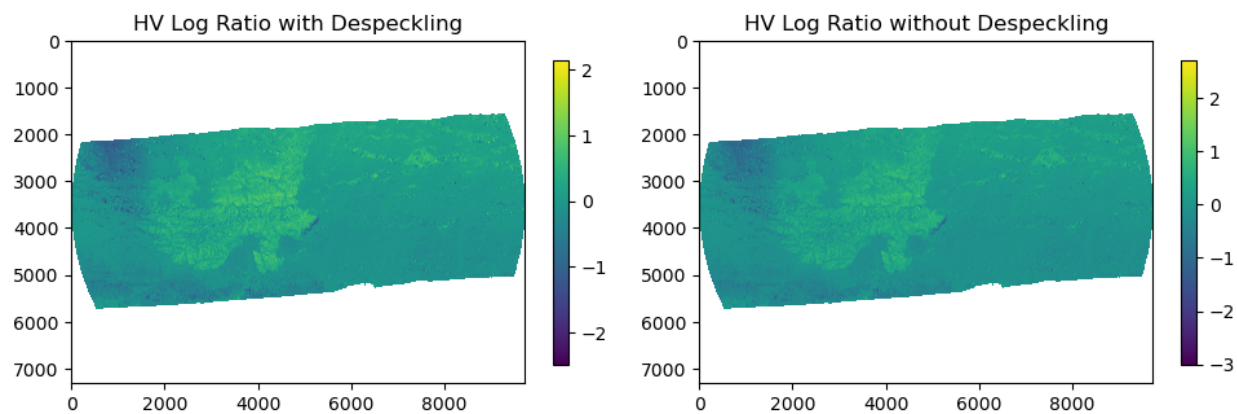


Figure 7. Comparison of interpolated Bobcat South image with (left) and without (right) total variation denoising.

SAR images often come with additive noise, which creates random variations that could be distracting and affect the classification outputs. To remove the noise, Chambolle's total

variation (TV) algorithm implemented by scikit-image is applied to the image as it is known to effectively perform noise reduction while persevering edges and fine details [17][18]. The denoised image (*Figure 7 left*) is a blurred version of the original image (*Figure 7 right*) and could be further blurred by changing the weight for Chambolle's algorithm at the expense of fidelity to image.

Superpixel Segmentation

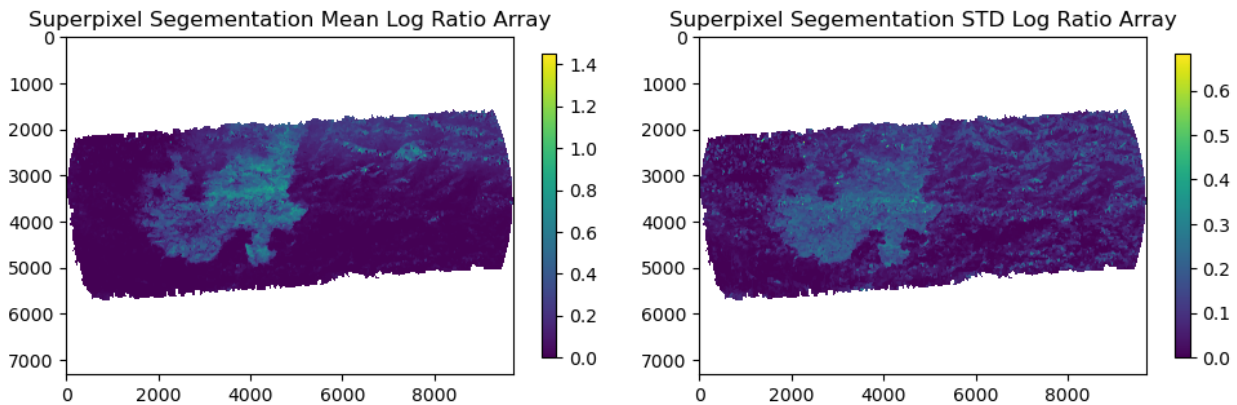


Figure 8. Feature extraction using superpixel segmentation. Mean (left) and Standard Deviation (right) Log Ratio of each superpixel is extracted and assigned to all the pixels within the superpixel.

Due to the large amount of pixels in the UAVSAR image, superpixel segmentation, using the Felzenszwalb's algorithm implemented on scikit-image, is performed to group pixels that share similar characteristics into larger segments, called superpixel [18][19]. This approach helps reduce the computational complexity by reducing the number of pixels needed to be processed and serves as a tool for feature extraction by considering the superpixels as units. For our product, the mean and standard deviation (STD) of HV Log Ratio is extracted within each segment to serve as features for classification. *Figure 8* shows the images where each pixel is populated with the mean/STD of the superpixel it belongs to, and highlights the fire areas (brighter areas). Note that for perimeter generation, Log Ratios (< 0) that represent vegetation gain are clipped to 0 to remove the noise from vegetation gain as we are only interested in

vegetation decrease (fire). Meanwhile, the vegetation gains are not clipped for the burn severity generation to ensure data accuracy.

Perimeter Mapping

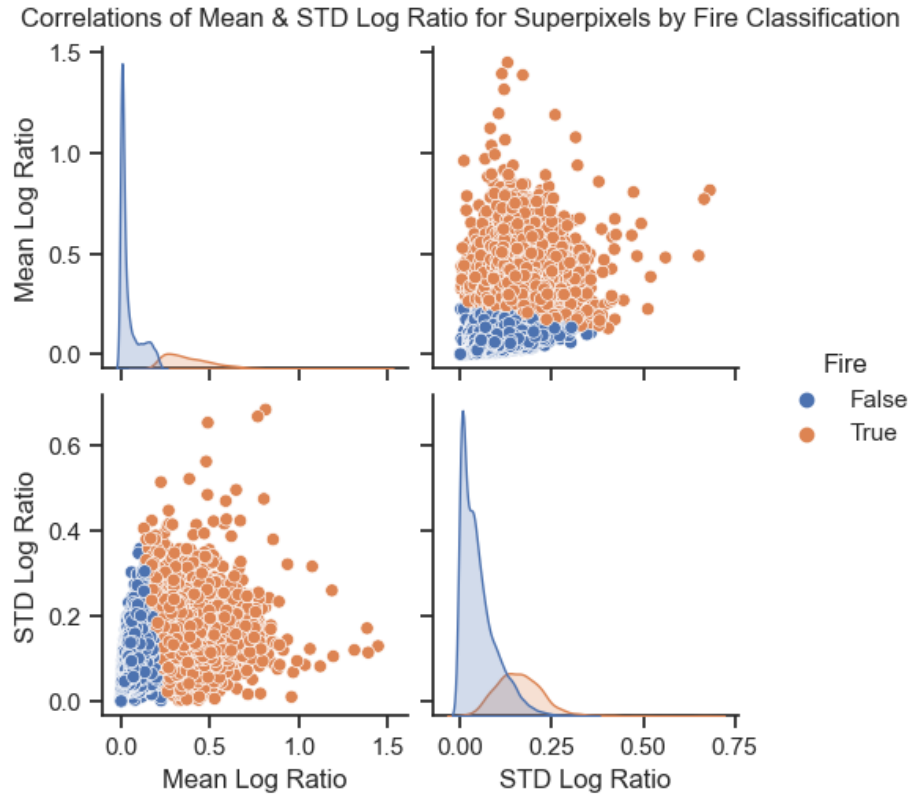


Figure 9. Correlation Plot of Mean and Standard Deviation HV Log Ratio based on the generated fire classification.

To distinguish burned areas using the two extracted features, the Lloyd's algorithm for K-Means clustering implemented by scikit-learn is selected for its simplicity and computational efficiency [14][20]. The dataset is clustered into 2 classes (fire and non-fire). *Figure 9* illustrates the distribution of mean log ratio and STD log ratio based on the clustering output using these two features. When comparing mean values of superpixels, a distinct separation between fire and non-fire regions is evident. On the other hand, the distribution of STD values shows some overlap, yet it offers supplementary insights, especially in distinguishing values near the boundary of these two classes. By considering the plot of STD versus mean (or mean versus

STD), a reasonable linear line is delineated to separate the two classes based on these two features. As a result, K-Means is a good fit for our data.

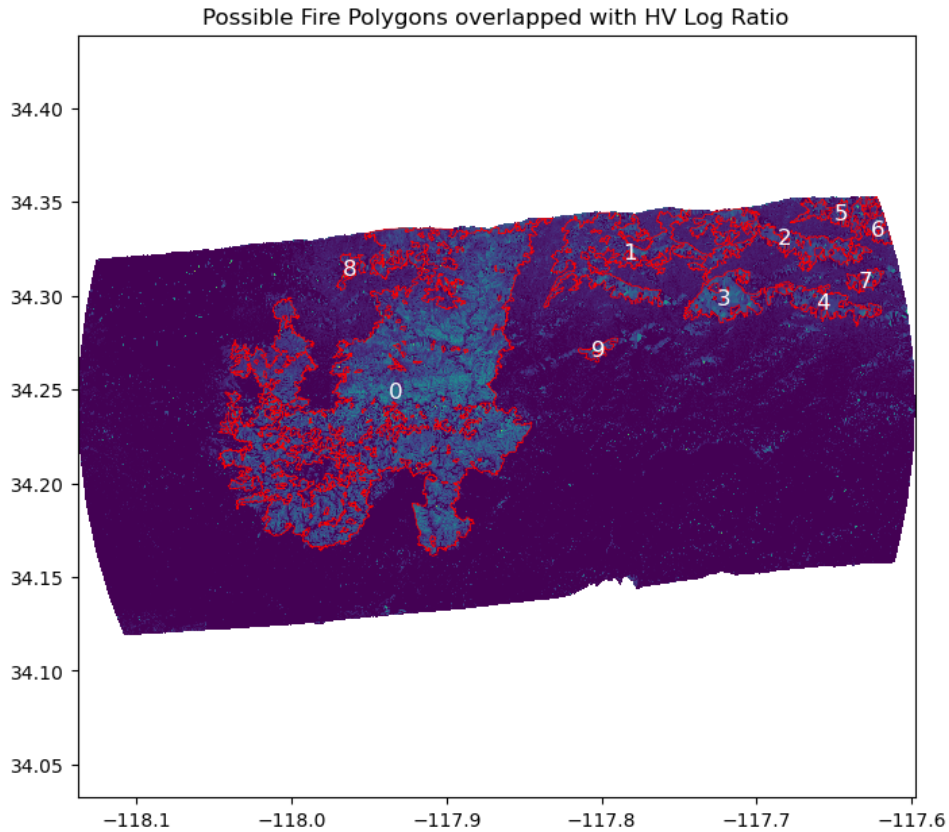


Figure 10. Polygon Selection plot for users to make informed decision about fire areas.

Upon classifying the superpixels into classes, the labels are assigned to each pixel within the superpixel to obtain the original shape. During post-processing, contiguous pixel labels are grouped as polygons for use as a GeoDataFrame that stores class labels and geometry of the pixels. The labels (0, 1) are organized such that classes with the higher mean HV Log Ratio, indication of fire, will always be assigned ‘1’ to simplify filtering. Polygons are filtered by area in user-specified square kilometer to remove false positive fire polygons. And the top 10 largest filtered polygons are returned for user to decide what to keep as part of the final perimeter. The

polygons are overlayed with the Mean HV Log Ratio to provide more context for the user during the polygon selection step (*Figure 10*).

Burn Severity Mapping

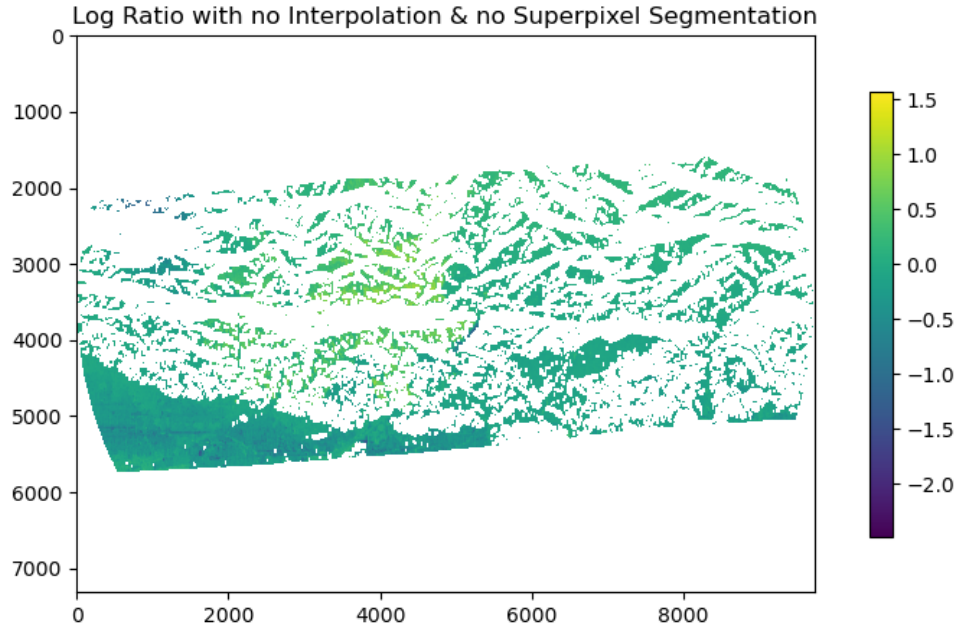


Figure 11. HV Log Ratio mapping for burn severity. Does not include interpolation and superpixel segmentation.

A simple approach is taken to classify burn severities into unburned, low, moderate, and high. Unlike the perimeter mapping, the burn severity mapping does not involve superpixel segmentation in order to reduce data loss due to the existence of missing values. This method uses the K-Means algorithm to classify the individual pixels into the four severity classes based on the distribution of the pixels' HV Log Ratio. The labels (1, 2, 3, 4) are assigned based on the mean Log Ratio for each class, such that the classes with higher mean Log Ratios are assigned higher label values to achieve a consistent labeling order across all product outputs: {1: Unburned, 2: Low, 3: Moderate, 4: High}.

This product is entirely open-sourced, and all the steps described in the **Methods** section are documented with the corresponding Python code and Jupyter Notebook sample in the GitHub repository.

Experiments

Other approaches were attempted during the product development process. These include but are not limited to the following.

Analysis was conducted using clustering techniques applied to a Pauli RGB color composite image. This composite image integrated the HH, HV, and VV polarizations into a single image to enhance the interpretation of different scattering mechanisms. However, this approach was discontinued due to the suboptimal outputs compared to that of HV polarization.

Instead of HV Log Ratio, difference and percent change between pre- and post- fire backscatter values were also considered. However, Log Ratio was ultimately chosen due to its capability to capture the maximum extent of fire area relative to the baseline perimeter.

In addition to experimenting with clustering algorithms, an alternative approach involving supervised learning utilizing the random forest classifier was explored. This included the manual creation of training labels using the baseline fire perimeter and the raster image of the log ratio. However, this method was abandoned due to concerns related to the size of the available training labels as they are manually created.

Finally, due to the distinct visual patterns present in the HV Log Ratio around perimeter edges, an experimentation with the Canny edge detection algorithm was carried out. The methods produced similar outcomes like the K-Means algorithm, but this approach introduced a considerable amount of noise into the resulting output. To address this issue, morphological

dilation and erosion techniques from the OpenCV were applied. However, this noise reduction approach led to the loss of feature detail outlining the fire edges.

Limitations and Future Works

The methods used in this product include some uncertainties and could be improved upon further research. One particularly significant limitation revolves around the scope of the sample fires we investigated. Although the product is designed to be applicable for any wildfires with UAVSAR data, it is only developed through analysis of three wildfires.

Additionally, the post-RTC UAVSAR image contains large amount of missing data due to terrain shadows. The current solution is the nearest neighbor interpolation which is sensitive to the location and the surrounding of the missing values. As discussed in the **Methods** section, this approach might not have a large impact on the perimeter generation, but has severe consequences for burn severity mapping, which leaves the severity output with missing data as a result of no interpolation. This problem could be approached by looking into and generalizing the terrain features of fires, and developing an interpolation approach for each type of terrain to improve data accuracy.

Although K-Means is a good choice of algorithm to start off, it is sensitive to the initial centroid selection, which could lead to suboptimal clustering solutions. K-Means also assumes equal cluster sizes and shapes, which does not reflect the true distribution of a typical UAVSAR image as generally more of the data contain non-fire areas. These two concerns about K-Means have a large impact on the burn severity generation because centroids are inconsistent due to different data distribution of different fires.

A possible solution for the inconsistent centroid problem is looking into various wildfire UAVSAR data and their mean HV Log Ratio distribution for each severity class. An analysis

could be done to determine the optimal centroid locations to initialize the 4 clusters for any wildfire. This method was initially attempted for the three fires but discontinued due to unreasonable distribution of centroids: for Station and La Tuna fires, the computed mean log ratio of a lower severity class was larger than the computed mean log ratio of a higher severity class. The method could be reapproached differently for further research. On the other hand, further research on HV Log Ratio or other polarimetric data could also be done to search for potential threshold values to divide both burned areas and burn severity. This approach will significantly reduce the runtime of the product due to its simplicity. Both solutions described require analysis on an extensive number of wildfires while this product is primarily developed using Bobcat Fire data.

Conclusion

As the frequency of wildfires continues to rise, gaining a comprehensive understanding of fire behavior and post-fire analysis has become crucial for making well-informed decisions. This proposed product develops a streamlined process that begins with preprocessing raw UAVSAR Polarimetric data, which exhibits remarkable sensitivity to detect variations in vegetation fuel load linked to fire events. Using the preprocessed data, the product can generate a GIS-compatible fire perimeter and burn severity map to reduce the manual efforts needed in the tradition methods of fire mapping. With enough data, the perimeter generation function could also be used to generate fire progression map. Our product provides timely and accurate insights based on the input UAVSAR data and enables decision-makers to make informed fire management strategies.

References

- [1] “Wildfire Climate Connection” *National Oceanic and Atmospheric Administration*, [Online]. Available: <https://www.noaa.gov/noaa-wildfire/wildfire-climate-connection>
- [2] Moritz, M., Batllori, E., Bradstock, R. *et al.* “Learning to coexist with wildfire.” *Nature* **515**, 58–66 (2014). <https://doi.org/10.1038/nature13946>
- [3] “What is Remote Sensing?” NASA Earthdata, [Online]. Available: <https://www.earthdata.nasa.gov/learn/backgrounder/remote-sensing>
- [4] “What is Synthetic Aperture Radar?” NASA Earthdata, [Online]. Available: <https://www.earthdata.nasa.gov/learn/backgrounder/what-is-sar>
- [5] An, K., Jones, C. E, Lou, Y. “Developing a detection and monitoring framework for wildfire regimes with L-Band Polarimetric SAR,” ESS Open Archive, Apr. 2023, doi: 10.22541/essoar.168056839.98485943/v1.
- [6] Kolden, C.A., Weisberg, P.J. Assessing Accuracy of Manually-mapped Wildfire Perimeters in Topographically Dissected Areas. *fire ecol* **3**, 22–31, Jun. 2007, doi: 10.4996/fireecology.0301022
- [7] Polarimetry | Get to Know SAR. (n.d.), NASA-ISRO SAR Mission (NISAR), [Online]. Available: <https://nisar.jpl.nasa.gov/mission/get-to-know-sar/polarimetry/>
- [8] “Wildfires: How can SAR detect vegetation changes throughout the wildfire cycle?” NASA-ISRO SAR Mission (NISAR), Mar. 2023, [Online]. Available: <https://storymaps.arcgis.com/stories/4724cd32c4064b9eb5ebe300c1385d07>
- [9] Flores, A., Herndon, K., Thapa, R.B., Cherrington, E. “The SAR Handbook: Comprehensive Methodologies for Forest Monitoring and Biomass Estimation,” pp 116-119, Apr. 2019, doi: 10.25966/nr2c-s697.
- [10] Dataset: UAVSAR, NASA. Retrieved from ASF DAAC. Accessed June 2023.
- [11] MTBS Data Access: Fire Level Geospatial Data. MTBS Project (USDA Forest Service/U.S. Geological Survey).[Online]. Accessed June 2023. Available: <http://mtbs.gov/direct-download>
- [12] Landsat Missions | United States Geological Survey (USGS), [Online]. Available: <https://www.usgs.gov/landsat-missions>
- [13] Mapping Methods | Monitoring Trends in Burn Severity (MTBS), [Online]. Available: <https://www.mtbs.gov/mapping-methods>

- [14] Lloyd, S., "Least squares quantization in PCM," in *IEEE Transactions on Information Theory*, vol. 28, no. 2, pp. 129-137, March 1982, doi: 10.1109/TIT.1982.1056489.
- [15] Simard, M., Riel, B. V., Denbina, M., Hensley, S., "Radiometric Correction of Airborne Radar Images Over Forested Terrain With Topography," in *IEEE Transactions on Geoscience and Remote Sensing*, vol. 54, no. 8, pp. 4488-4500, Aug. 2016. doi: 10.1109/TGRS.2016.2543142
- [16] Denbina, M., Hawkins, B., Nuemann, M., "Kapok: Python Library for PolInSAR Forest Height Estimation Using UAVSAR Data," Jul. 2017, doi: 10.5281/zenodo.833487
- [17] Chambolle, A., "An Algorithm for Total Variation Minimization and Applications," *Journal of Mathematical Imaging and Vision* **20**, 89–97, Jan. 2004, doi: 10.1023/B:JMIV.0000011325.36760.1e
- [18] Van der Walt S, Schönberger JL, Nunez-Iglesias J, et al. "scikit-image: image processing in Python," PeerJ 2:e453, Jun. 2014, doi: 10.7717/peerj.453
- [19] Felzenszwalb, P.F., Huttenlocher, D.P., "Efficient Graph-Based Image Segmentation," *International Journal of Computer Vision* **59**, 167–181, Sep. 2004, doi: 10.1023/B:VISI.0000022288.19776.77
- [20] Pedregosa F, Varoquaux G, Gramfort A, et al, "Scikit-learn: Machine Learning in Python," *Journal of Machine Learning Research*, Vol 12, pp 2825-2830, Nov. 2011, doi: 10.5555/1953048.2078195

Acknowledgements

I would like to thank my mentors Karen An and Charlie Marshak for their constant support and guidance throughout the entire duration of the project. Their consistent availability and willingness to address my questions has prevented me from going down many rabbit holes and directed me to the final solutions. Thank you, Karen, for your insights into the wildfire behaviors and explanations of outcomes relative to the fire. Thank you, Charlie, for addressing all my technical inquiries and guiding me towards existing functions and algorithms to explore.

Thank you to everyone in group 334F for cultivating a welcoming and inclusive environment for me. The atmosphere made me excited to head into office every day to engage in enjoyable and educational conversations. Thank you to Yang Zheng and Yunling Lou from 334F for sponsoring this project. I would also like thank individuals I met from JPL SUDS community's Ask a Data Scientist office hour for also helping me with my technical approach and suggesting new directions.

Lastly, thank you to family and friends for their constant support and encouragement this Summer! And thank you, JPL, for this amazing opportunity!